Measurements of dispersion forces between colloidal latex particles with the atomic force microscope and comparison with Lifshitz theory

Magdalena Elzbieciak-Wodka,[1] Mihail N. Popescu,[2] F. Javier Montes Ruiz-Cabello,[1] Gregor Trefalt,[1] Plinio Maroni,[1] and Michal Borkovec[1,a)]

[1]*Department of Inorganic and Analytical Chemistry, University of Geneva, Sciences II, 30, Quai Ernest-Ansermet, 1205 Geneva, Switzerland*

[2]*Ian Wark Research Institute, University of South Australia, Mawson Lakes, SA 5095, Australia*

(Received 18 December 2013; accepted 21 February 2014; published online 12 March 2014)

Interaction forces between carboxylate colloidal latex particles of about 2 μm in diameter immersed in aqueous solutions of monovalent salts were measured with the colloidal probe technique, which is based on the atomic force microscope. We have systematically varied the ionic strength, the type of salt, and also the surface charge densities of the particles through changes in the solution pH. Based on these measurements, we have accurately measured the dispersion forces acting between the particles and estimated the apparent Hamaker constant to be $(2.0 \pm 0.5) \times 10^{-21}$ J at a separation distance of about 10 nm. This value is basically independent of the salt concentration and the type of salt. Good agreement with Lifshitz theory is found when roughness effects are taken into account. The combination of retardation and roughness effects reduces the value of the apparent Hamaker constant and its ionic strength dependence with respect to the case of ideally smooth surfaces. [http://dx.doi.org/10.1063/1.4867541]

I. INTRODUCTION

The theoretical framework to calculate forces between electrically neutral macroscopic bodies based on their dielectric spectra was developed by Lifshitz and co-workers almost 50 years ago.[1–3] This theory generalized the earlier work of van der Waals, which focussed on non-retarded forces at small distances, and the one of Casimir and Polder, treating retardation effects that are important at larger separation distances. While such forces are being associated with any of the names mentioned, we will refer to dispersion forces here. These forces are typically attractive, but they can be repulsive for certain combination of materials.[1,4–7] Dispersion forces control adhesion between surfaces, aggregation, or deposition rates of colloidal particles, or attachment of particles to air bubbles in mineral flotation processes.[1,4,5,8–10] These forces are attracting renewed interest, especially in the development of microelectromechanical systems or low friction devices.[3,7,11]

Detailed comparison between experiment and theory was hampered for a long time. On the theoretical side, there was a lack of information on the dielectric spectra of the materials involved over a sufficiently wide frequency range. Nowadays, accurate dielectric spectra are available for a wide range of materials, and thus dispersion forces can be calculated without adjustable parameters.[12–15] On the experimental side, the surface forces apparatus permitted first reliable measurements of dispersion forces in the crossed cylinder geometry.[1,16] More recently, torsional devices[17,18] or total internal reflection microscopy (TIRM)[19,20] were used to measure dispersion forces between a spherical particle and a planar substrate. Closed-loop atomic force microscopes (AFMs) made the measurements of these forces possible with the colloidal probe technique.[6,7,12,21]

The Lifshitz theory of dispersion forces has been experimentally validated in various systems. Symmetric systems investigated featured attractive forces and included gold surfaces across vacuum[17,18] or liquids[12] as well as polystyrene[20] or titania[22] across water. The asymmetric systems studies involve silica and mica surfaces across water[23] as well as gold/poly(tetrafluoroethylene)[6] or gold/silica[7] across organic solvents. In the latter two systems, repulsive dispersion forces were reported. Discrepancies between experiment and theory were attributed to surface roughness, residual charges, or both.[3,12,18,20] Measurements of dispersion forces between individual particles in solution proved to be difficult. Forces between colloidal particles were measured with optical tweezers and video microscopy, but the technique is not easily applicable for attractive potentials.[24] Forces between colloidal particles can be also measured with the AFM-based colloidal probe technique, whereby the second particle is attached to the substrate and aligned with the one on the cantilever.[25–27] Attractive forces between zinc sulphide particles were reported, but they featured an unusually strong dependence on the salt level.[25] Earlier measurements of dispersion forces between polystyrene latex particles proved unsuccessful[26] due to interferences by capillary interactions between nanosized bubbles.[28] More recently, measurements of dispersion forces involving latex particles were carried out with newly developed multi-particle colloidal probe technique by some of us.[29–31] This technique permits to attach particles to the AFM-cantilever and to the substrate in solution without drying.[29,32] Another complication is that dispersion forces in aqueous

a)Author to whom correspondence should be addressed. Electronic mail: michal.borkovec@unige.ch, Tel.: + 41 22 379 6053.

solutions are often masked by strong double layer forces. At higher salt concentrations or at lower charge densities, however, double layer forces weaken and the measured interactions between the particles can be captured by a superposition of double layer and dispersion forces. This superposition principle represents the basis of the classical theory of Derjaguin, Landau, Verwey, and Overbeek (DLVO).[33]

Here we use the multi-particle colloidal probe technique to measure the interaction forces between individual polystyrene latex particles across monovalent salt solutions. The present studies address various ionic strengths, types of salt, and surface charge densities, and thereby substantially extend earlier measurements of dispersion forces by TIRM.[20] The force profiles are quantitatively interpreted within DLVO theory, which allows us to determine the contribution due to dispersion interactions. The observed dispersion forces are significantly weaker than the ones expected from Lifshitz theory for smooth surfaces. However, this situation can be rationalized quantitatively by accounting for roughness.

II. CALCULATION OF FORCES BETWEEN PARTICLES

This section summarizes the calculation of the interactions between spherical particles across an aqueous electrolyte solution. Within the classical DLVO picture, the force F between two particles at a surface separation distance h can be decomposed as[33]

$$F(h) = F_{\mathrm{dl}}(h) + F_{\mathrm{dis}}(h), \tag{1}$$

where $F_{\mathrm{dl}}(h)$ is the double layer force and $F_{\mathrm{dis}}(h)$ the dispersion force. We adopt the Derjaguin (or proximity) approximation that relates the force to the interaction energy per unit area $\Phi(h)$ in the following fashion:[33]

$$F(h) = 2\pi R_{\mathrm{eff}} \Phi(h), \tag{2}$$

where the effective radius is given by

$$R_{\mathrm{eff}} = \frac{R_1 R_2}{R_1 + R_2}, \tag{3}$$

where R_1 and R_2 are the radii of the two spheres. This procedure introduces a substantial simplification for the theoretical modelling, since one deals with the plate-plate geometry only. By comparing Lifshitz calculations in the plate-plate and sphere-sphere geometries for polystyrene, the Derjaguin approximation was shown to be valid for particles with diameters above 0.5 μm up to separations of 100 nm within 1%.[33,34]

The double layer force $F_{\mathrm{dl}}(h)$ in monovalent electrolytes can be obtained accurately within the Derjaguin approximation by solving the Poisson-Boltzmann equation analytically or numerically.[35,36] At large separations, the double layer force decays exponentially. The range of this force is given by the Debye length κ^{-1}, which is related to the salt concentration as[33]

$$\kappa^2 = \frac{2e^2 N_{\mathrm{A}} I}{kT\varepsilon(0)}, \tag{4}$$

where e is the elementary charge, N_{A} is the Avogadro's number, I is the ionic strength, k is the Boltzmann constant, T is the absolute temperature, and $\varepsilon(0)$ is the (static) dielectric constant of water. At shorter distances, the force profile depends explicitly on the boundary conditions. We adopt the constant regulation approximation, which introduces an additional regulation parameter p. The frequently used constant charge (CC) and constant potential (CP) boundary correspond to $p = 1$ and $p = 0$, respectively. In the general case, this parameter can adopt any value $p \leq 1$.[35–37]

The calculation of the dispersion force $F_{\mathrm{dis}}(h)$ will be described in the following. First we summarize the Lifshitz theory that is used to calculate the retarded dispersion interaction between smooth surfaces, and then we discuss how the effect of roughness is introduced.

A. Lifshitz theory

The non-retarded (van der Waals) dispersion interaction energy between two semi-infinite plates is given by[33]

$$\Phi(h) = -\frac{A}{12\pi h^2}, \tag{5}$$

where A is the Hamaker constant. We will use Eq. (5) to analyse the experimental force profiles in an approximate fashion.

The Lifshitz theory introduces retardation effects due to finite velocity of the propagation of electromagnetic fields and predicts that the dispersion force has a more complex dependence on the separation distance. This dependence is typically accounted for by introducing an effective Hamaker parameter, which becomes a function of the separation h. By analogy to Eq. (5), this effective Hamaker parameter is defined as[33]

$$A_{\mathrm{eff}}(h) = -12\pi h^2 \Phi(h). \tag{6}$$

In the non-retarded case, the effective Hamaker parameter corresponds to the Hamaker constant A. For the free energy $\Phi(h)$ per unit area of two parallel flat dielectric plates (half-spaces) separated by another dielectric medium we use the formulation of Mahanty and Ninham of the classical Lifshitz's theory and write[33,38]

$$\Phi(h) = \frac{kT}{2\pi}\left[\frac{1}{2}\int_0^\infty dq\, q \ln\left[\phi_0(q;h)\right] + \sum_{n=1}^{\infty}\int_0^\infty dq\, q \ln\left[\phi(q;i\xi_n,h)\right]\right], \tag{7}$$

where q is the magnitude of the wave vector with units of inverse length, $\xi_n = 2\pi n kT/\hbar$ with n being the summation index, $\hbar$ is Planck's constant, and

$$\phi(q;i\xi,h) = \left[1 - \left(\frac{\bar{t}-t}{\bar{t}+t}\right)^2 e^{-2th}\right] \times \left[1 - \left(\frac{\bar{\varepsilon}(i\xi)/\bar{t} - \varepsilon(i\xi)/t}{\bar{\varepsilon}(i\xi)/\bar{t} + \varepsilon(i\xi)/t}\right)^2 e^{-2th}\right], \tag{8}$$

with the abbreviations $t = \sqrt{q^2 + \xi^2\varepsilon^2(i\xi)/c^2}$ and $\bar{t} = \sqrt{q^2 + \xi^2\bar{\varepsilon}^2(i\xi)/c^2}$, while c denotes the speed of light in vacuum and $i = \sqrt{-1}$. The permittivity functions

$\varepsilon(\omega)$ and $\bar{\varepsilon}(\omega)$ refer to the solid material and the liquid in between, respectively, and they have to be known as a function of the angular frequency ω. The zero frequency term is given by

$$\phi_0(q;h) = 1 - \left[\frac{\bar{\varepsilon}(0)/s - \varepsilon(0)/q}{\bar{\varepsilon}(0)/s + \varepsilon(0)/q}\right]^2 \exp(-2\,s\,h), \qquad (9)$$

where $s = \sqrt{q^2 + \kappa^2}$ and κ is the inverse Debye length defined in Eq. (4). The latter expression accounts for the effects of salt, when the medium separating the two half spaces is a dilute electrolyte rather than a perfect dielectric. Mahanty and Ninham[33,38] have shown that response of free ionic charges contributes significantly only to the $n = 0$ (static) component. The above expressions are evaluated numerically by truncating sums at $n = 300$. The accuracy of this approximation in the relevant separation range of 0.1 nm $\leq h \leq$ 1000 nm was tested by doubling the number of terms in the sum and is about 1%. The frequency dependent permittivity functions $\varepsilon(i\xi)$ and $\bar{\varepsilon}(i\xi)$ for aqueous electrolyte solutions and polystyrene are approximated as[33]

$$\varepsilon(i\xi),\ \ \bar{\varepsilon}(i\xi) = 1 + \sum_j \frac{d_j}{1 + \xi\tau_j} + \sum_k \frac{f_k}{1 + g_k\,\xi/\omega_k + (\xi/\omega_k)^2}, \qquad (10)$$

where we used the parameters d_j, τ_j, f_k, g_k, and ω_k as tabulated in the book by Russel *et al.*[33] on page 141. Figure 1(a) shows the calculated dependence on the surface separation h of the effective Hamaker parameter $A_{\text{eff}}(h)$ for smooth surfaces for the two ionic strengths of 1 mM and 1 M. The curves corresponding to these two values delimitate from above and below the grey shaded region in Fig. 1(a). For any salt concentration between these two values, the corresponding curves $A_{\text{eff}}(h)$ lie within this region.

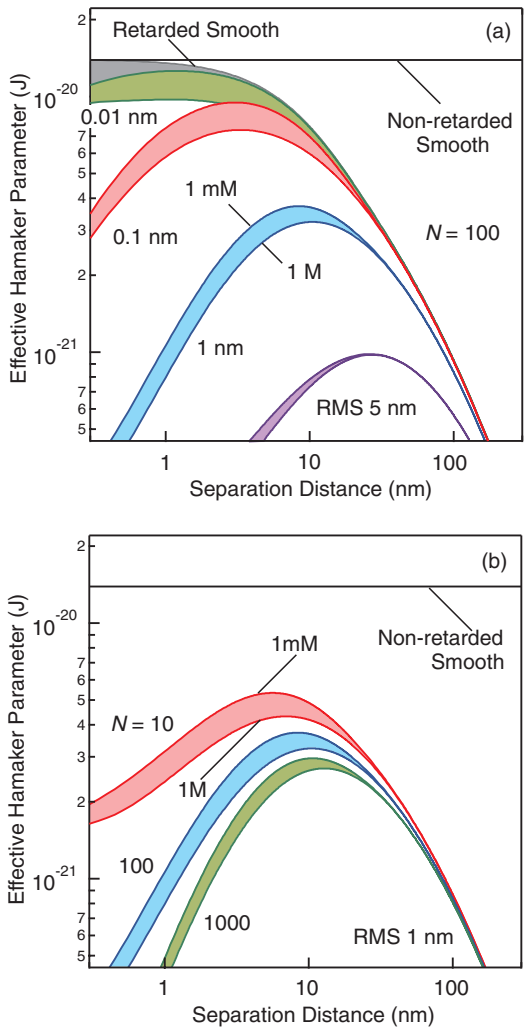

FIG. 1. Effective Hamaker parameter versus the surface separation distance h calculated with the Lifshitz theory including roughness described by a Gaussian height distribution. The figure compares force profiles at two different salt concentrations of 1 mM and 1 M, and the shaded areas indicate the region of the location of the profiles with concentrations in between. The various shaded regions correspond to various root mean square (RMS) roughness and different number N of discrete pillars. The latter number characterizes the ratio between the areas of the interaction zone and of individual topographic features on the surface. (a) The effect varying the RMS roughness for fixed $N = 100$. The results for smooth surfaces are shown in grey. (b) The effect varying of the number N of pillars for fixed RMS of 1 nm.

B. Roughness effects on dispersion forces

Various studies have addressed effects of roughness on dispersion forces.[18,20,39–43] Our calculations rely on the Derjaguin approximation, which is expected to be applicable to surfaces of moderate roughness. The calculation proceeds in two steps. The first step calculates the interaction between a finite set of imaginary pillars with random heights arranged on a finite contact zone of surface S, while the second step averages over independent realizations of the random heights of these pillars.[43] With these assumptions, the dispersion force between two rough spheres can be expressed as

$$F_{\text{dis}} = 2\pi\,R_{\text{eff}}\langle\Phi^{(\text{r})}[D(x,y)]\rangle = 2\pi\,R_{\text{eff}}\left\langle\iint_s \frac{dx\,dy}{S}\Phi_{\text{pp}}(D(x,y))\right\rangle, \qquad (11)$$

where $\Phi^{(r)}$ denotes the free energy per unit area of two rough plates as a functional of the separation-distribution $D(x,y)$ at locations with the lateral Cartesian coordinates x, y, Φ_{pp} is the plate-plate interaction energy per unit area for smooth surfaces, and the average $\langle ... \rangle$ denotes the ensemble average. The separations $D(x,y)$ are determined by the height distributions of $h_1(x,y)$ and $h_2(x,y)$, which both obey the same probability distribution, since the statistical properties of both particle surfaces are expected to be the same. The integral in Eq. (11) can be calculated by discretization by means of individual surface area elements. The size of one element reflects the size of a typical topographic feature (i.e., height-height correlation length) and Eq. (11) can be therefore further approximated as

$$F_{\text{dis}} = 2\pi\,R_{\text{eff}}\left\langle\sum_{i=1}^{N}\frac{\Phi_{\text{pp}}(D_i)}{N}\right\rangle, \qquad (12)$$

where i runs over the number of area elements pairs at coordinates x_i and y_i in which the surface is discretized,

$D_i = D(x_i,y_i)$, and the average is taken over various realizations $\{D_i\}_{i=1,\ldots,N}$.

Equation (12) is used to calculate dispersion interactions between rough surfaces. In practice, the calculation proceeds as follows. For a given height distribution, one can generate two sets of height profiles with N elements each, $\{h_{1,i}\}_{i=1,\ldots,N}$ and $\{h_{2,i}\}_{i=1,\ldots,N}$, which represent the discretization of two rough surfaces into a collection of pillars at each surface area element. The point of mechanical contact is determined for the index i at which the summed heights are maximal, namely,

$$h_{1,c} + h_{2,c} = \max\{h_{1,i} + h_{2,i}\}_{i=1,\ldots,N}. \quad (13)$$

Observing that $h_{1,i} + h_{2,i} + D_i$ is independent of the index i, the local separations are obtained in terms of the surface separation h as

$$D_i = h + h_{1,c} + h_{2,c} - h_{1,i} - h_{2,i}. \quad (14)$$

The sum in Eq. (12) is then computed for all separations of interest with the expression for Φ_{pp} corresponding to the various cases considered. The steps above are repeated for different realizations of the sets of heights $\{h_{1,i}\}_{i=1,\ldots,N}$ and $\{h_{2,i}\}_{i=1,\ldots,N}$. We have normally used 100 realizations and for few cases it was checked that doubling the number of realizations does not lead to substantial changes. For fixed h, the results of various realisations are then averaged to finally obtain the interaction forces.

In order to estimate the interaction between two similar spherical, rough colloids, by means of the procedure described above, the height distribution and the number of pillars N must be known. For illustration purposes, we have used a Gaussian distribution of zero mean, which is thus completely characterized by the standard deviation, the latter also being referred to as root mean square (RMS) roughness. We have equally varied the number of pillars N in the relevant interaction zone to investigate the effect of the correlation length. The area occupied by each pillar corresponds to the square of the height-height correlation length, while the area of the interaction zone represents the surface area, which contributes substantially to the interaction. The number of pillars N thus reflects the ratio between the area of interaction zone and the area of each pillar.

Figure 1 shows the calculated effective Hamaker parameter as a function of the separation distance. Figure 1(a) illustrates the effect of varying the RMS of the roughness at a fixed number of pillars $N = 100$ in the relevant interaction zone. The important qualitative feature is that while for a smooth surface the effective Hamaker parameter decreases monotonically, for a rough surface it actually passes through a maximum. This feature indicates that at small separations, the dispersion forces between rough surfaces are weaker than the ones between smooth ones.[43] Second observation is that the effective Hamaker parameter decreases with increasing RMS of the roughness. This behaviour can be intuitively understood since in the presence of roughness, the contact is determined by a small number of asperities, while large parts the surfaces are not in contact. This gap effectively increases the actual separation and consequently reduces the dispersion force. This effect is most pronounced at short separation distances, while it becomes unimportant when the surfaces are widely separated. The third notable consequence of roughness is that it diminishes the dependence of the dispersion interactions on the ionic strength. For smooth surfaces, the salt dependence is significant at small separations, but it becomes negligible when the separation is increased above roughly 10 nm. Since roughness reduces the dispersion interactions at short separations, this effect also eliminates the contributions, which would have had induced significant ionic strength dependence the force. Therefore, the dependence on the ionic strength is reduced. While an increase in the ionic strength from 1 mM to 1 M may reduce the dispersion force by about 35% for a smooth surface at surface separations below 1 nm, the maximum reduction is only about 15% for RMS of 1 nm, and this effect is hardly noticeable for RMS of 5 nm. Figure 1(b) shows the influence of the number of pillars N in the relevant interaction zone on the effective Hamaker parameter for RMS of 1.0 nm. Increasing the number of pillars decreases the strength of the interaction, even though the effect is relatively weak compared to that due to increasing RMS. This reduction can be understood as follows. When N is increased, the tail of the roughness distribution is sampled more effectively, and therefore the terms with larger local separation contribute more strongly. This reduction will be most noticeable at small N, where finite-size effects in sampling the height distribution are significant.

III. EXPERIMENTAL

A. Materials

Carboxyl-terminated surfactant-free polystyrene latex particles were obtained as an aqueous suspension from Interfacial Dynamic Corporation (Portland, OR). The diameter of the particles was 1.94 μm and the polydispersity index was 9.7% as determined by transmission electron microscopy by the manufacturer. The carboxyl latex particle suspensions were dialyzed against pure water with a cellulose membrane having a molecular mass cut-off of 300 kg/mol (Spectrum). The experiments were carried out with suspensions of a particle concentration around 80 mg/l. All solutions were prepared with Milli-Q water adjusted to pH 3.0, 4.0, and 5.6 with HCl (Sigma-Aldrich) and to the desired ionic strength by adding monovalent salt. The measurements were carried out with KCl, KSCN (Acros Organics), and CsCl (Sigma-Aldrich). Dissolved gases were removed from the electrolyte solutions with a Gastorr degasser during 1 h at 100 mbar. The pH was checked after the experiment and remained constant. Experiments were carried out at room temperature of $23 \pm 2\,^{\circ}$C.

B. Force measurements

The multi-particle colloidal probe technique was used to measure the interaction forces between latex particles immersed in monovalent electrolyte solutions. The measurements were carried out with a closed-loop AFM (MFP-3D, Asylum Research) mounted on an inverted optical microscope (Olympus IX 70).

The glass plate that seals the AFM fluid-cell was cleaned for about 2 h in a piranha solution, which consists of a mixture of H_2SO_4 (98%) and H_2O_2 (30%) in a ratio 3:1. After rinsing with Milli-Q water and drying with nitrogen, the plate was cleaned for 20 min in air plasma (PDC-32G, Harrick, New York) and finally silanized with 3-(ethoxydimethylsilyl)propylamine (Sigma-Aldrich) in an evacuated container overnight. The cantilevers (μMasch, Tallin, Estonia) were directly cleaned in the air plasma and silanized in the same fashion. The fluid cell was sealed with the silanized glass plate and the particle suspension was injected into the cell. The particles were left to adhere to the substrate for about 2 h. The particles that did not adhere to the substrate were removed by rinsing the cell with the same degassed electrolyte solution as the one used to suspend the particles. Subsequently, a colloidal spherical particle was picked up with the AFM cantilever. The attachment is sufficiently strong to prevent rotational motions of the particles, even though small librations upon approach cannot be excluded. Such librations may lead to more attractive force profiles. The attached particle was centred above another particle on the substrate and the alignment was checked through the interference fringes observed with the optical microscope. The alignment has a lateral precision of better than 0.1 μm. The interaction forces were obtained by averaging about 150 approach and retraction cycles, which were accumulated with a sampling rate of 5 kHz, a cycling frequency of 0.5 Hz, and approach-retraction velocities of 300 nm/s. For these velocities, effects of hydrodynamic interactions are negligible. While these forces increase upon approach, they are only about 3 pN at a distances 2 nm. After a measurement sequence, the particle used was detached and another particle was attached to the cantilever. Forces were measured for at least 3 pairs of particles, and the results showed good reproducibility between the different pairs. This finding indicates that large scale surface heterogeneities do not play an important role. The zero separation was obtained from the onset of the constant compliance region with a precision of about 0.5 nm. The cantilever deflection was converted into force through the spring constant of the cantilever. The cantilever spring constants were in the range of 0.15–0.3 N/m, and they were measured independently by analysing the thermal fluctuations of the cantilever[44] or by measuring its resonance frequency and its lateral dimensions.[45] Results agreed within 10% and the average of these results was used. The measured forces were finally normalized with the effective radius given by Eq. (3). The necessary diameters of the individual particles were obtained with the optical microscope with a precision of about 0.2 μm.

C. Imaging

Cypher-AFM (Asylum Research, Santa Barbara) was used to image the particles in solution with the amplitude modulation mode. Biolever mini cantilevers (AC40TS, Olympus, Japan) with a tip radius below 9 nm and a resonance frequency of 25–30 kHz were used.

Functionalized mica was chosen as the substrate. The functionalization was achieved by incubating for 5 min the freshly cleaved mica sheets in a solution of linear poly(ethylene imine) (Polysciences) of molecular mass around 2.5 kg/mol, polymer concentration of 55 mg/l, and pH 4.6. The surface was then rinsed with water and dried in a stream of nitrogen. The particles were deposited from a particle suspension in 1 mM KCl solution of pH 5.6 at a particle concentration around 200 mg/l. The substrate was incubated in the suspension during 15 min, and the particles that did not adhere to the substrate were removed by rinsing the mica surface with pure electrolyte solution.

Images were acquired with a scan rate of 0.5 μm/s, a free oscillation amplitude (FOA) of about 20 nm, and a set point corresponding to around 70% of the FOA. The cantilever spring constant was 0.09 N/m as measured through thermal fluctuations. The RMS roughness of 15 particles was determined by imaging the topography of an area of 0.5 $\times$ 0.5 μm^2 on the surface of each particle.

D. Electrophoresis

Electrophoretic mobilities of the latex particles in suspension was determined with laser Doppler velocimetry (Zetasizer Nano ZS, Malvern Instruments, UK). The same electrolyte solutions were used as for the direct force measurements. The electrophoretic mobility was converted into surface potentials with the standard electrokinetic model developed by O'Brien and White.[46] The single ion conductivities used in the model of 7.35 S/m/M for K^+, 7.77 S/m/M for Cs^+, 7.64 S/m/M for Cl^-, and 6.60 S/m/M for SCN^- were taken from literature.[47]

IV. RESULTS AND DISCUSSION

Force profiles and electrophoretic mobility of negatively charged carboxylated latex particles were measured in different monovalent salt solution and various pH values. These conditions permitted to investigate eventual specific effects dependent on the type of ions present and on the surface charge density. The latter parameter could be tuned since the degree of ionization of the carboxylic groups depends strongly on solution pH.

A. Particle imaging

Particle surfaces were imaged in an electrolyte solution with the AFM in the amplitude modulation mode. Typical images are shown in Fig. 2. The particles are rather smooth, but some residual asperities can be systematically observed. These asperities might represent the precursor particles that have formed during the synthesis process.[48] The height distribution of these asperities was always close to a normal distribution, see Fig. 2(c). The RMS roughness did vary somewhat from particle to particle. Analysing about 15 images, we found an average RMS roughness of 1.1 nm with a standard deviation of about 0.4 nm. The correlation length was estimated from the radially averaged height-height correlation

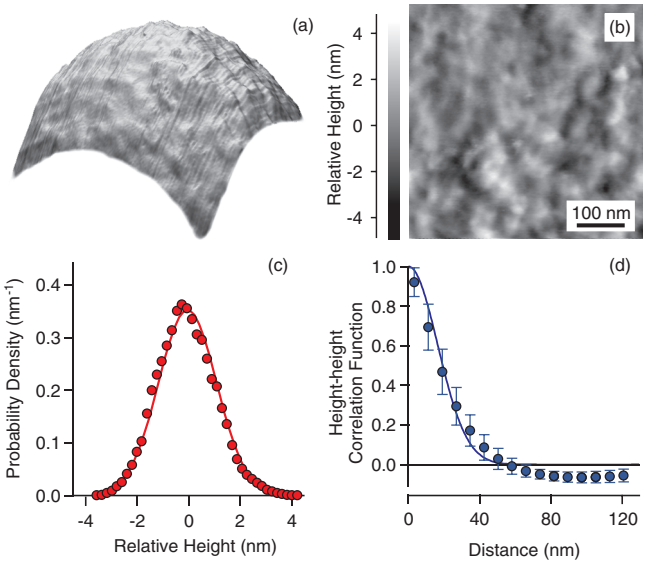

FIG. 2. AFM imaging in solution of the latex particles used. (a) Spherical cap image and (b) the corresponding flattened topographic image with the corresponding gray-scale for the height. (c) The measured relative height distribution with respect to its mean together with a Gaussian best fit. (d) Measured average height-height correlation function together with a Gaussian best fit at small distances.

function, which was calculated from the images. The normalized correlation function did not show any systematic differences between different particles. To reduce the noise, the correlation functions calculated from the images were averaged over different particles and the result is shown in Fig. 2(d). The decay at short distances can be well described with a Gaussian with a standard deviation of 16.3 nm, which we identify as the correlation length. This model breaks down at larger distances, where the correlation function indicates a weak oscillation and becomes negative. Since only an approximate estimate of the correlation length is needed, a more detailed analysis of this correlation function was not attempted.

B. Colloidal probe force measurements

Forces between individual particles were measured with the colloidal probe technique based on the AFM. Typical results at different concentrations of KCl electrolyte and various pH values are shown in Fig. 3. At pH 5.6, the particles are highly charged and the forces are all repulsive except at 500 mM, which is the highest ionic strength investigated (Fig. 3(a)). At pH 4.0, the particles are less charged and attraction sets in already at an ionic strength of 80 mM (Fig. 3(b)). At pH 3.0, the particles are very weakly charged, and the interactions become attractive already at ionic strengths above 20 mM (Fig. 3(c)).

At larger distances, the force profiles can be accurately interpreted with classical DLVO theory, and therefore they convey substantial details on dispersion forces. Thereby, the profiles were fitted with a superposition of non-retarded dispersion forces as given in Eq. (5) and double layer interactions. The latter forces were calculated with the Poisson-Boltzmann equation subject to constant regulation boundary condition. At smaller distances, typically below 3 nm, the measured forces are more attractive than the behaviour predicted by DLVO theory. In this regime, however, the actual force profile cannot be measured due to the jump-in

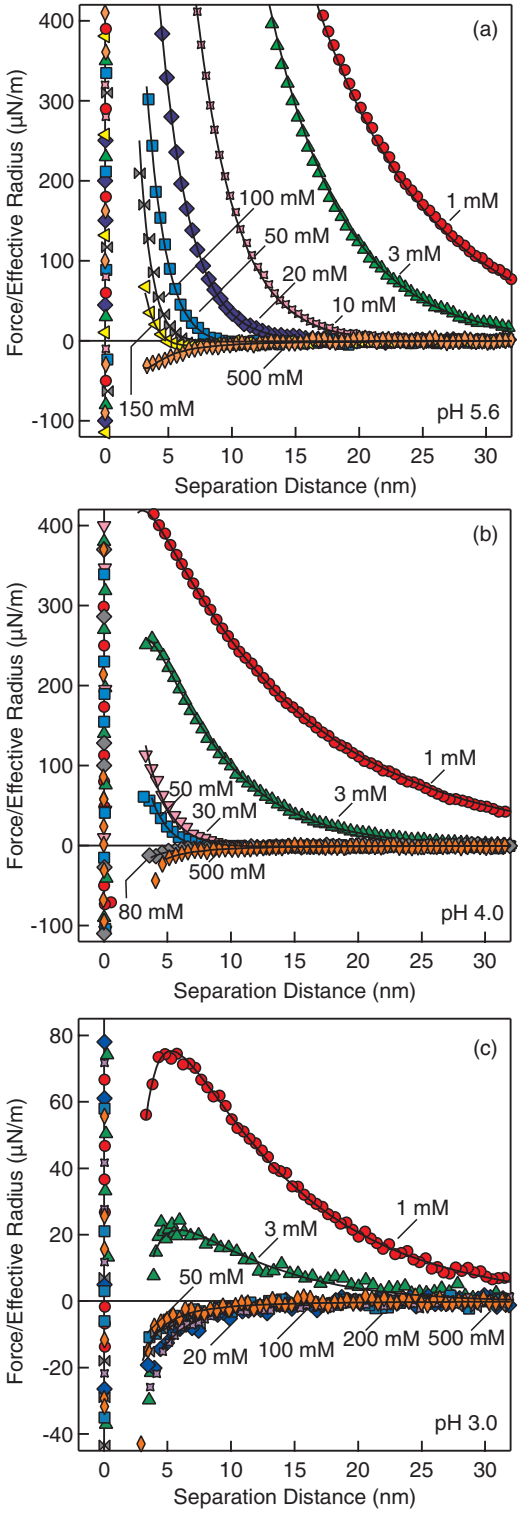

FIG. 3. Colloidal probe AFM force measurements between carboxylated latex particles normalized to the effective radius versus the separation distance. The measurements were carried out in KCl electrolyte solutions of different ionic strength. Solid lines are best fits with DLVO theory. (a) pH 5.6, (b) pH 4.0, and (c) pH 3.0.

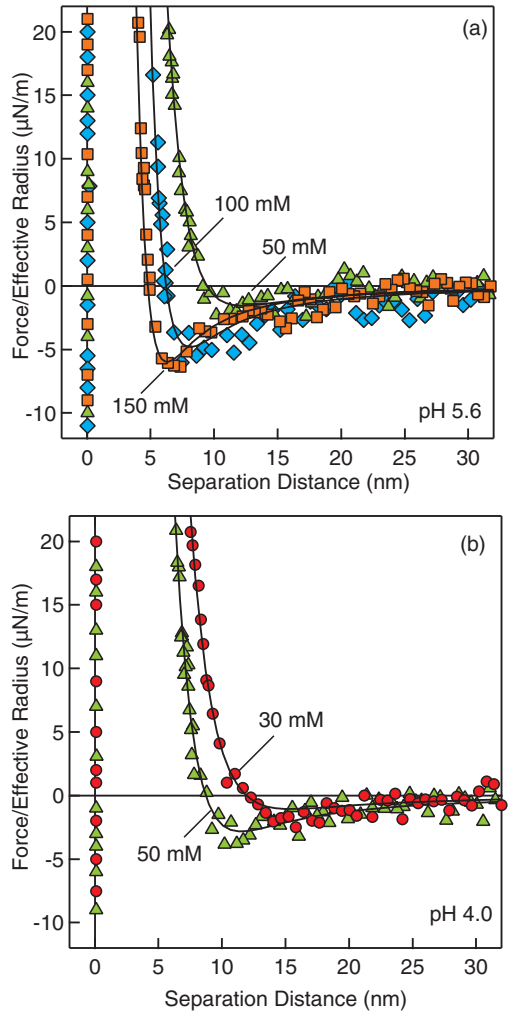

FIG. 4. Colloidal probe AFM force measurements between carboxylated latex particles normalized to the effective radius versus the separation distance. The measurements were carried out in KCl electrolyte solutions of different ionic strength. Solid lines are best fits with DLVO theory. The figure represents a zoom into Figure 3 such that the minima in the force become visible. (a) pH 5.6 and (b) pH 4.0.

instability of the cantilever. The additional attractive forces probably originate from hydrophobic interactions, discrete charge effects, patch-charge interactions or combinations thereof.

At intermediate ionic strengths, where the magnitudes of repulsive and attractive forces become comparable, one observes a minimum in the force profiles, typically at distances of 5–15 nm. This minimum can only be clearly seen once we zoom into Fig. 3. The relevant profiles are replotted on a smaller scale in Fig. 4. This minimum in the force is related to the so-called secondary minimum in the energy profile,[33] which is located where the force profile passes through zero. The shape of the force profiles in the vicinity of this minimum is particularly sensitive to all parameters entering in the DLVO calculation. Therefore, by fitting these profiles one obtains reliable estimates for the Hamaker constant.

Fitting the force profiles with the DLVO theory yields the diffuse layer surface potential ψ_d, the regulation parameter p, the actual ionic strength I, and the Hamaker constant A. The ionic strength and the regulation parameter could be only obtained from force profiles that feature strong double layer interactions. The ionic strength was always within 10% of the value known from the solution composition, and subsequently it was fixed to the latter value. From subsequent fits of the force profiles the regulation parameter varies somewhat, and one obtains $p = 0.49 \pm 0.02$. This parameter was finally fixed to $p = 0.49$, and all force curves were refitted with this value. One thus obtains the surface potential and the Hamaker constant. The non-retarded expression for the dispersion force was sufficient to obtain a good fit of the measured force profiles. For purely attractive forces, the surface potential and the Hamaker constant could be also extracted from the fit with confidence, provided the ionic strength was fixed to the known value obtained from the solution composition. The estimates of the surface potential and the Hamaker constant obtained in this manner are discussed in Subsections IV C and IV D.

C. Electrostatic surface potentials

Figure 5(a) shows the dependence of the surface potentials on the KCl concentration that were obtained by fitting the force profiles. They are compared with surface potentials estimated from electrophoresis (ζ-potentials). The force profiles depend solely on the magnitude of the potential, but not on its sign. The negative sign of these potentials is assigned such that they agree with the ζ-potentials obtained from electrophoresis. The negative sign is also compatible with the carboxylic groups at the particle surface, which become negatively charged when they dissociate in solution. One observes good agreement between the potentials measured by AFM and by electrophoresis, especially at small magnitudes. At higher magnitudes, the electrophoresis results tend to yield larger magnitudes than the potentials obtained from the force measurements. Similar deviations between surface potentials of latex particles measured by AFM and electrophoresis were reported in other systems.[31,49] Deviations between these two techniques might be related to surface charge heterogeneities, which would induce additional rotational motion of the particles.[50]

The same measurements were carried out in KSCN and CsCl salt solutions, and the corresponding surface potentials were shown in Figs. 5(b) and 5(c). The results are similar to the ones observed in the KCl salt solution. No specific ion effects were found.

The magnitude of the surface potentials increases with increasing ionic strength and increasing pH. The ionic strength dependence can be rationalized relatively well with the Gouy-Chapman equation, which relates the surface charge density σ and the diffuse layer potential ψ_d for an isolated charged interface as

$$\psi_d = \frac{2kT}{e}\operatorname{arcsinh}\left(\frac{e\sigma}{2kT\kappa\varepsilon_0\varepsilon(0)}\right). \quad (15)$$

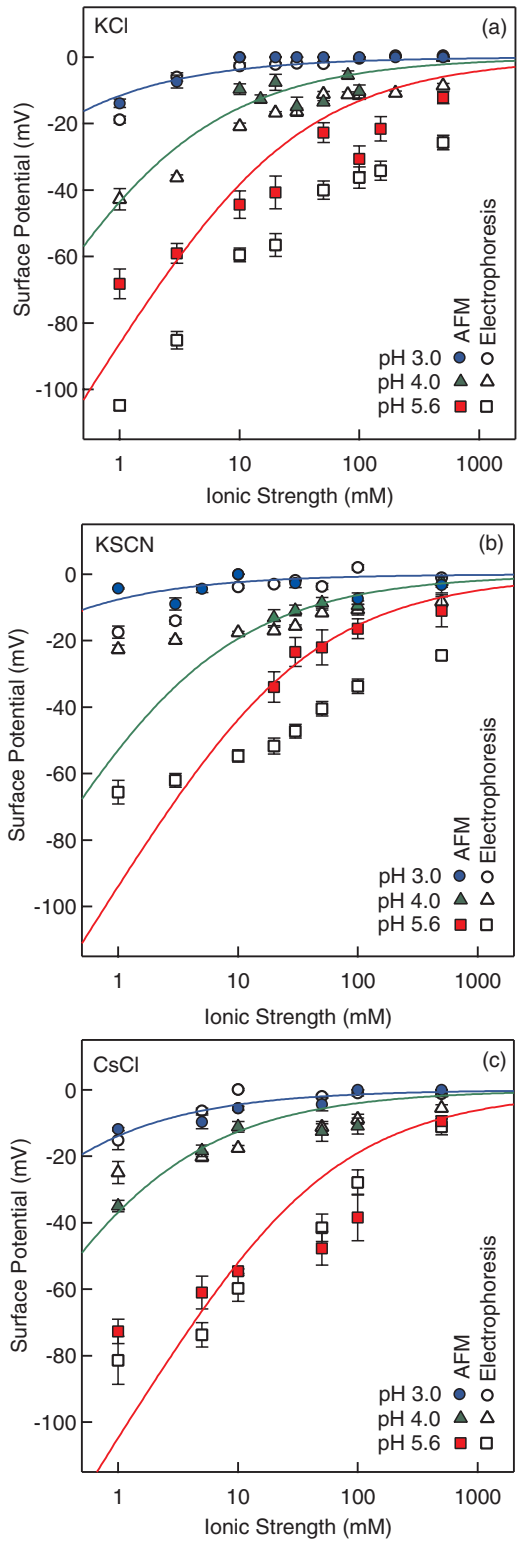

FIG. 5. Electrostatic surface potentials versus the ionic strength at different pH as determined from the DLVO fit of the force profiles measured with the AFM and ζ-potentials determined from electrophoresis. Solid lines are calculations based on the Gouy-Chapman model. (a) KCl, (b) KSCN, and (c) CsCl.

The resulting surface charge densities are summarized in Table I. One observes that their magnitude increases with increasing pH, which can be rationalized with the increasing degree of ionization of the carboxylic surface groups. On the other hand, the surface charge densities do not depend on the type of monovalent salt.

TABLE I. Summary of fitted surface charge densities (mC/m^2) from the measured force profiles.

Salt	pH 3.0	pH 4.0	pH 5.6
KCl	–0.849	–3.55	–9.60
KSCN	–0.909	–4.54	–11.3
CsCl	–1.02	–2.90	–14.0

D. Effective Hamaker parameters

Hamaker constants obtained from best fits of the force profiles with DLVO theory involving non-retarded dispersion forces given by Eq. (5) are in the range of $(2.0 \pm 0.5) \times 10^{-21}$ J. These values are basically independent of the ionic strength, and they are substantially smaller than the non-retarded Hamaker constant of 14.0×10^{-21}J obtained from Lifshitz theory for smooth surfaces.[20,33] Consideration of the finite separation distance and screening by salt may eventually account for a 30%–50% reduction, but the resulting values still remain substantially larger than the measured one. On the other hand, roughness of the surface combined with retardation effects can explain this reduction in the effective Hamaker parameters.

To make a more precise comparison with the calculations, we have assigned to the determined Hamaker constants a particular separation distance h in the following fashion. When a minimum in the force was present, the determined Hamaker constant was associated to the distance of the minimum. For purely attractive curves, the attractive region was divided in two parts. Hamaker constants were then determined by fitting the DLVO profile to each of them, and the respective midpoints were taken as the relevant separations. These fitted Hamaker constants were thus identified with the effective Hamaker parameters at the respective distance.

The theoretical curves were obtained from Lifshitz theory including roughness as described in Sec. II. The height distribution was assumed to be Gaussian, which represents a very good approximation to the experimentally determined height distributions as illustrated in Fig. 2(c). The RMS roughness was taken to be equal to the average of 1.1 nm from several images. The number of pillars was estimated from the ratio between the area of the interaction zone and the base area of a pillar. The latter was calculated from the height-height correlation length of 16.3 nm to be about 266 nm^2. The interaction area was obtained by considering the surface area S of two overlapping imaginary shells around each particle of radius R_{eff} of thickness $\bar{h}$, where $\bar{h}$ corresponds to the average range of the interaction. Provided $\bar{h} \ll R_{\text{eff}}$, this area can expressed as

$$S = 2\pi \bar{h} R_{\text{eff}}. \tag{16}$$

By taking the average range of the interaction $\bar{h} = 15$ nm with Eq. (16) one obtains an interaction area of about 45700 nm^2 and thus $N = 170$.

The dependence of the effective Hamaker parameter on the separation distance is compared with the experimental data in KCl electrolyte solutions in Fig. 6(a). We show the results of the calculation for two different ionic strengths, namely 1 mM and 1 M. The salt dependence is basically negligible in the present situation. For comparison, the results are shown of the respective calculations for RMS of the roughness values of 0.7 nm and 1.5 nm, which correspond to the mean plus or minus one standard deviation. Thereby, we present only the results of the calculation at 1 mM for the smaller RMS, while for 1 M for the larger RMS. Figure 6(a) confirms that Lifshitz theory with roughness effects can rationalize the experimentally observed effective Hamaker parameters in the relevant distance range of 5–20 nm rather well.

The most important uncertainty entering the calculation is the variation in the roughness from particle to particle, which leads to the substantial spread in the calculated curves as indicated in Fig. 6(a). The dependence on the number of pillars N as well as on the salt concentration is much weaker. The present calculations explain nicely why no ionic strength dependence of the effective Hamaker parameter is observed. For smooth surfaces, retarded dispersion forces are expected to show substantial ionic strength dependence at separations below 10 nm. As discussed in Sec. II, this dependence is strongly suppressed through the presence of roughness, which is in full agreement with experimental data.

The electrolytes KCl, KSCN, and CsCl were also investigated and the corresponding results are shown in Figs. 6(b) and 6(c). The results for the effective Hamaker parameters as well as its interpretation in terms of Lifshitz theory including roughness are virtually identical for these different salts. Similarly to double-layer forces, no specific ion effects on dispersion forces were found.

One might question an inconsistency in the data interpretation since the non-retarded dispersion force was used to fit the experimental data, but effects of retardation were used to interpret the observed values of the effective Hamaker parameters. Inspection of Fig. 6 reveals that the effective Hamaker parameter does depend on the separation distance, but it also reveals that this dependence is very weak. On the other hand, the experimental window where dispersion forces can be measured reliably is the relatively narrow separation range of 5–20 nm. The lower value is given by the resulting deviations from DLVO theory due to the presence of additional attractive forces and the jump-in instability of the cantilever. The upper value is dictated by the noise in the force measurement, which is around 3 pN. This range covers less than an order of magnitude in distances, and the expected variation in the effective Hamaker parameter is $<25\%$. Given the noise in the experiments, this variation is at the detection limit of the present setup. Therefore, the use of a non-retarded expression is justified and this approximation simplifies the data analysis substantially.

Once the surface potentials have been established, an alternative approach can be used to determine the effective Hamaker parameters. At sufficiently high ionic strength, the double layer component of the interaction force is negligible at larger separations to a good approximation. Therefore, the

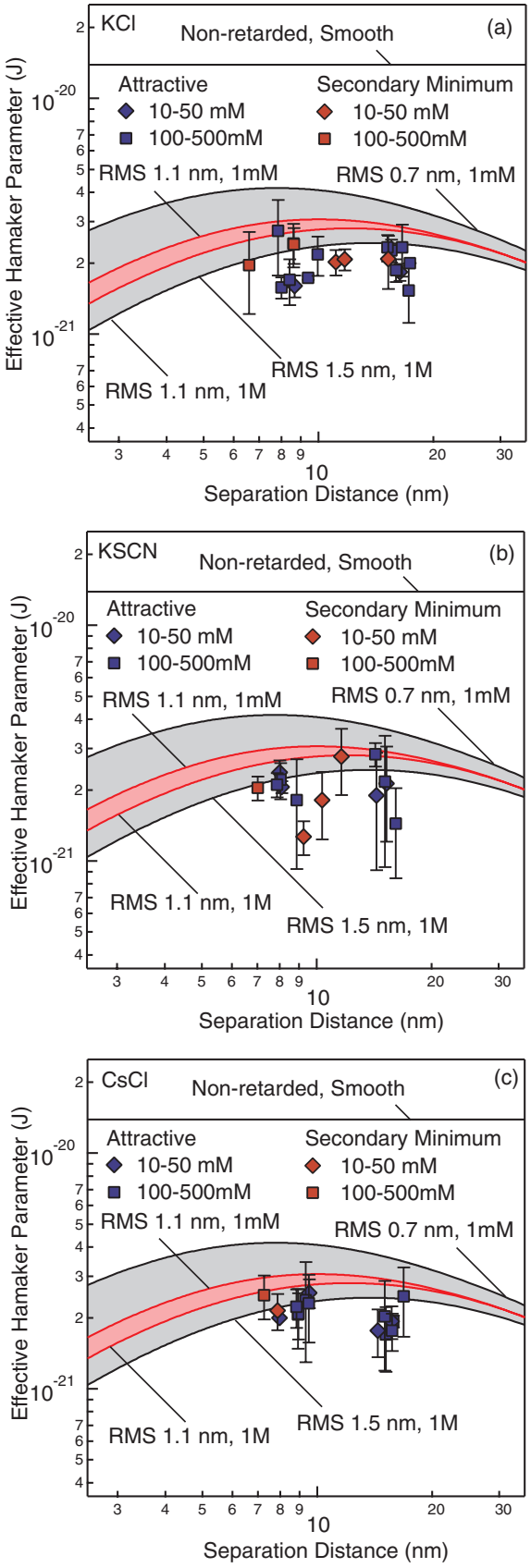

FIG. 6. Effective Hamaker parameters versus the separation distance for different experimental conditions, including overall attractive force profiles, and those featuring a secondary minimum. The ranges of the experimental ionic strengths are indicated. Solid lines are calculations based on Lifshitz theory with roughness at an ionic strength of 1 mM and 1 M. In all cases, $N = 170$ was used. (a) KCl, (b) KSCN, and (d) CsCl.

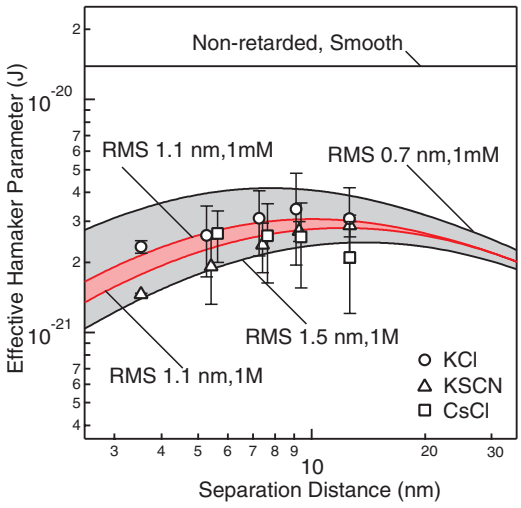

FIG. 7. Effective Hamaker parameters versus the separation distance obtained from force profiles at 500 mM and at pH 5.6 for different salts. Solid lines are calculations based on Lifshitz theory with and without roughness at an ionic strength of 1 mM and 1 M.

force profiles in this regime can be used to directly calculate the effective Hamaker parameter by means of Eqs. (2) and (6). Such results are presented in Fig. 7 for an ionic strength of 0.5 M and pH 5.6. Under these conditions, the contribution of the double layer force is about 2% at a distance of 4 nm. While the scatter of the data is substantial, one observes the trends are very similar as the ones reported in Fig. 6. This analysis further supports that the approach leading to the data shown in Fig. 6 is indeed consistent.

V. CONCLUSION

We have measured interaction forces between carboxylated colloidal latex particles of about 2 μm in diameter over a wide range of salt concentrations and surface charge densities. The Hamaker constant was estimated to be $(2.0 \pm 0.5) \times 10^{-21}$ J at a distance of about 10 nm. This value is in good agreement with the Lifshitz theory estimate when considering roughness effects. The combination of retardation and roughness effects substantially reduces the effective Hamaker parameter from the value expected for smooth surfaces and supresses the ionic strength dependence of the dispersion forces. These features are in full agreement with experiment.

ACKNOWLEDGMENTS

This research was supported by the Swiss National Science Foundation, University of Geneva, COST Action CM1101, and Swiss Secretariat of Education and Research. M.N.P. acknowledges a travel grant from the Australian Academy of Science within the mentioned COST Action.

[1]J. Israelachvili, *Intermolecular and Surface Forces* (Academic Press, London, 1992).
[2]E. Elizalde and A. Romeo, Am. J. Phys. **59**, 711–719 (1991).
[3]G. L. Klimchitskaya, U. Mohideen, and V. M. Mostepanenko, Rev. Mod. Phys. **81**, 1827–1885 (2009).
[4]R. F. Tabor, R. Manica, D. Y. C. Chan, F. Grieser, and R. R. Dagastine, Phys. Rev. Lett. **106**, 064501 (2011).
[5]K. L. Chen and M. Elimelech, Environ. Sci. Technol. **42**, 7607–7614 (2008).
[6]A. Milling, P. Mulvaney, and I. Larson, J. Colloid Interface Sci. **180**, 460–465 (1996).
[7]J. N. Munday, F. Capasso, and V. A. Parsegian, Nature (London) **457**, 170–173 (2009).
[8]M. Kobayashi, M. Skarba, P. Galletto, D. Cakara, and M. Borkovec, J. Colloid Interface Sci. **292**, 139–147 (2005).
[9]L. Parkinson and J. Ralston, J. Phys. Chem. C **114**, 2273–2281 (2010).
[10]H. I. Petrache, T. Zemb, L. Belloni, and V. A. Parsegian, Proc. Natl. Acad. Sci. U.S.A. **103**, 7982–7987 (2006).
[11]P. J. van Zwol and G. Palasantzas, Adv. Sci. Lett. **3**, 358–362 (2010).
[12]J. N. Munday, F. Capasso, V. A. Parsegian, and S. M. Bezrukov, Phys. Rev. A **78**, 032109 (2008).
[13]P. J. van Zwol, G. Palasantzas, and J. T. M. De Hosson, Phys. Rev. B **79**, 195428 (2009).
[14]P. J. van Zwol and G. Palasantzas, Phys. Rev. A **81**, 062502 (2010).
[15]J. L. Li, J. Chun, N. S. Wingreen, R. Car, I. A. Aksay, and D. A. Saville, Phys. Rev. B **71**, 235412 (2005).
[16]J. N. Israelachvili and G. E. Adams, J. Chem. Soc. Farad. Trans. I **74**, 975–1001 (1978).
[17]S. K. Lamoreaux, Phys. Rev. Lett. **78**, 5–8 (1997).
[18]R. S. Decca, E. Fischbach, G. L. Klimchitskaya, D. E. Krause, D. Lopez, and V. M. Mostepanenko, Phys. Rev. D **68**, 116003 (2003).
[19]D. C. Prieve, Adv. Colloid Interface Sci. **82**, 93–125 (1999).
[20]M. A. Bevan and D. C. Prieve, Langmuir **15**, 7925–7936 (1999).
[21]U. Hartmann, Phys. Rev. B **43**, 2404–2407 (1991).
[22]I. Larson, C. J. Drummond, D. Y. C. Chan, and F. Grieser, J. Am. Chem. Soc. **115**, 11885–11890 (1993).
[23]P. G. Hartley, I. Larson, and P. J. Scales, Langmuir **13**, 2207–2214 (1997).
[24]M. Brunner, J. Dobnikar, H. H. von Grunberg, and C. Bechinger, Phys. Rev. Lett. **92**, 078301 (2004).
[25]G. Toikka, R. A. Hayes, and J. Ralston, Langmuir **12**, 3783–3788 (1996).
[26]R. F. Considine, R. A. Hayes, and R. G. Horn, Langmuir **15**, 1657–1659 (1999).
[27]S. Rentsch, R. Pericet-Camara, G. Papastavrou, and M. Borkovec, Phys. Chem. Chem. Phys. **8**, 2531–2538 (2006).
[28]X. H. Zhang, A. Quinn, and W. A. Ducker, Langmuir **24**, 4756–4764 (2008).
[29]I. Popa, P. Sinha, M. Finessi, P. Maroni, G. Papastavrou, and M. Borkovec, Phys. Rev. Lett. **104**, 228301 (2010).
[30]P. Sinha, I. Szilagyi, F. J. Montes Ruiz-Cabello, P. Maroni, and M. Borkovec, J. Phys. Chem. Lett. **4**, 648–652 (2013).
[31]M. Finessi, P. Sinha, I. Szilagyi, I. Popa, P. Maroni, and M. Borkovec, J. Phys. Chem. B **115**, 9098–9105 (2011).
[32]I. Popa, G. Gillies, G. Papastavrou, and M. Borkovec, J. Phys. Chem. B **114**, 3170–3177 (2010).
[33]W. B. Russel, D. A. Saville, and W. R. Schowalter, *Colloidal Dispersions* (Cambridge University Press, Cambridge, 1989).
[34]B. A. Pailthorpe and W. B. Russel, J. Colloid Interface Sci. **89**, 563–566 (1982).
[35]S. H. Behrens and M. Borkovec, J. Phys. Chem. B **103**, 2918–2928 (1999).
[36]R. Pericet-Camara, G. Papastavrou, S. H. Behrens, and M. Borkovec, J. Phys. Chem. B **108**, 19467–19475 (2004).
[37]M. Borkovec and S. H. Behrens, J. Phys. Chem. B **112**, 10795–10799 (2008).
[38]J. Mahanty and B. W. Ninham, *Dispersion Forces* (Academic Press, New York, 1976).
[39]W. Broer, G. Palasantzas, J. Knoester, and V. B. Svetovoy, EPL **95**, 30001 (2011).
[40]G. Bimonte, T. Emig, R. L. Jaffe, and M. Kardar, EPL **97**, 50001 (2012).
[41]A. Gusso and U. B. Reis, EPL **99**, 36003 (2012).
[42]P. J. van Zwol, V. B. Svetovoy, and G. Palasantzas, Phys. Rev. B **80**, 235401 (2009).
[43]M. Kruger, V. A. Golyk, G. Bimonte, and M. Kardar, EPL **104**, 41001 (2013).
[44]J. L. Hutter and J. Bechhoefer, Rev. Sci. Instrum. **64**, 1868–1873 (1993).
[45]J. E. Sader, J. W. M. Chon, and P. Mulvaney, Rev. Sci. Instrum. **70**, 3967–3969 (1999).

[46]R. W. O'Brien and L. R. White, J. Chem. Soc. Faraday Trans. 2 **74**, 1607–1626 (1978).
[47]A. L. Horvath, *Handbook of Aqueous Electrolyte Solutions: Physical Properties, Estimation, and Correlation Methods* (Ellis Horwood, Chichester, 1985).
[48]M. E. Dobrowolska, J. H. Van Esch, and G. J. M. Koper, Langmuir **29**, 11724–11729 (2013).
[49]F. J. Montes Ruiz-Cabello, P. Maroni, and M. Borkovec, J. Chem. Phys. **138**, 234705 (2013).
[50]J. L. Anderson, J. Colloid Interface Sci. **105**, 45–54 (1985).